Acta Geochim (2022) 41(3):419–433
https://doi.org/10.1007/s11631-022-00538-x

ORIGINAL ARTICLE

Rare earth element (REE) geochemistry of different colored fluorites from the Baoshan Cu–Pb–Zn deposit, Southern Hunan, South China

Jinchuan Huang[1] · **Jiantang Peng**[2]

Received: 4 October 2021 / Revised: 8 March 2022 / Accepted: 10 March 2022 / Published online: 25 April 2022

Abstract The Baoshan Cu–Pb–Zn deposit, located in the central part of the Qin–Hang belt in South China, is closely related to the granodiorite-porphyry. However, the characteristics and the source of the ore-forming fluid are still ubiquitous. According to the crosscutting relationships between veinlets and their mineral assemblages, three stages of hydrothermal mineralization in this deposit were previously distinguished. In this contribution, two different colored fluorites from the major sulfide mineralization stage are recognized: (1) green fluorites coexisting with Pb–Zn ores; and (2) violet fluorites coexisting with pyrite ores. Y/Ho ratios verify the green fluorites and violet fluorites were co-genetic. The fluorites display elevated $(La/Yb)_N$ ratios, which decrease from 1201 to 5710 for green fluorites to 689–1568 for violet fluorites, indicating that they precipitated at the early hydrothermal sulfide stage, and Pb–Zn ores crystallized earlier than pyrite ores. The similar Tb/La ratios of the fluorites also indicate that they precipitated at an early stage within a short time. From the green fluorites to violet fluorites, the total rare earth element (ΣREE) concentrations decrease from 1052–1680 ppm to 148–350 ppm, indicating that the green fluorites precipitated from a more acidic fluid. The Eu/Eu* ratios increase from 0.17 to 0.30 for green fluorites to 0.29–0.48 for violet fluorites, and the Ce/Ce* ratios decrease from 1.08–1.13 to 0.93–1.11, suggesting a gradual increase in oxygen fugacity (fO_2) and pH value of the mineralization fluid. Though the fluorites display similar REE patterns to the granodiorite-porphyry and limestone, the ΣREE concentrations of the fluorites are significantly higher than those of limestone and the granodiorite-porphyry, suggesting that an important undetected non-magmatic source is involved to provide sufficient REE for fluorites. The most plausible mechanism is fluid mixing between magma fluid and an undetected non-magmatic fluid.

Keywords Trace element geochemistry · REE · Fluorite · Baoshan Cu–Pb–Zn deposit · Southern Hunan · South China

1 Introduction

Since the Mesozoic, large-scaled tectonic activity and widespread magmatism have happened in South China (Maruyama et al. 1997; Zhou et al. 2006), which gave rise to the emplacement of the voluminous granites and the formation of numerous associated W–Sn, Cu–Pb–Zn, and Nb–Ta deposits (Hua and Mao 1999; Hua et al. 2003; Li et al. 2013; Hu et al. 2017a, b). Among them, the large-scaled porphyry- and skarn-type Cu–Pb–Zn polymetallic deposits predominantly distributed along the Qinzhou–Hangzhou tectonic belt (Qin–Hang belt) (Fig. 1; Mao et al. 2011, 2013), making it one of the most important intracontinental Cu-polymetallic metallogenic belts in South China (Mao et al. 2011).

✉ Jiantang Peng
jtpeng@126.com

[1] The Key Laboratory of Solid Waste Treatment and Resource Recycle, Ministry of Education, Southwest University of Science and Technology, Mianyang 621010, People's Republic of China

[2] State Key Laboratory of Ore Deposit Geochemistry, Institute of Geochemistry, Chinese Academy of Sciences, Guiyang 550002, People's Republic of China

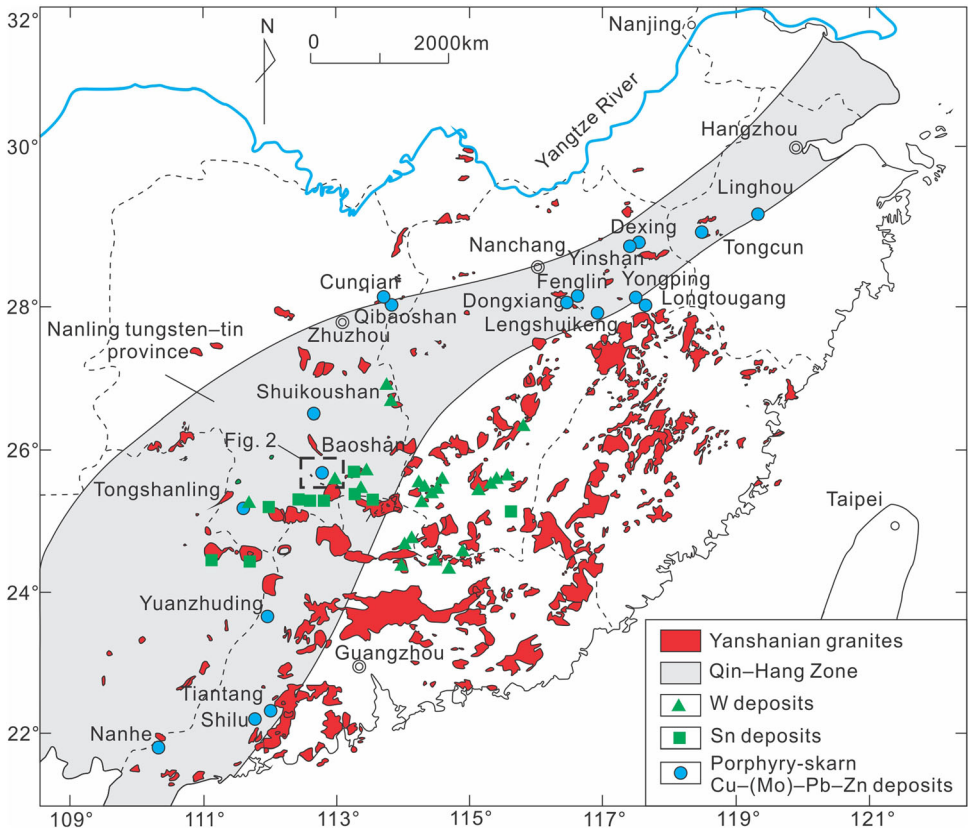

Fig. 1 Simplified geological mapping showing the distribution of Yanshanian granitoids in South China, the W-Sn polymetallic deposits in the Nanling district and Cu polymetallic deposits in the Qin–Hang belt. Modified after Zhou et al. (2006) and Mao et al. (2013)

The Baoshan Cu–Pb–Zn deposit in southern Hunan, located in the central part of the Qin–Hang belt (Zhou et al. 2012), is closely associated with the granodiorite-porphyry (Yao et al. 2006; Zhu et al. 2012; Xie et al. 2015; Ding et al. 2016; Zhang et al. 2018). As an important porphyry- and skarn-type Cu–Pb–Zn deposit in the Qin–Hang belt (Mao et al. 2011, 2013), Cu–Mo–Pb–Zn polymetallic mineralization widely occurs with obvious horizontal zoning around the granitoid (Xuan et al. 2017). It has become a focus of research on the sources of the ore-forming materials (Zhu et al. 2012; Bao et al. 2014; Xie et al. 2015; Ding et al. 2016; Xuan et al. 2017), the geochronology and petrogenesis of the related granitoids (Wang et al. 2003; Lu et al. 2006; Xie et al. 2013; Mi et al. 2018) in the recent years. However, the characteristics and the source of the ore-forming fluid are still ubiquitous and thus limited the understanding of the genesis of the Baoshan deposit.

Rare earth elements (REE) can be incorporated in a considerable amount into Ca-bearing minerals (such as fluorite, calcite, and scheelite) to substitute Ca^{2+} because of the similar ionic radius between Ca^{2+} and REE^{3+} (Elzinga et al. 2002). The fractionation among different REEs can be ascribed to the chemical complexation reactions, adsorption effects, and redox reactions involving Ce and Eu (e.g., Bau and Möller 1992; Bau and Dulski 1995; Schwinn and Markl 2005; Sasmaz et al. 2005a). Fluorite is not only an economically important mineral but also an important gangue mineral related to Pb–Zn, Cu, Ag, Mo, W, and Sn deposits (Sasmaz et al. 2005a, b; Sasmaz and Yavuz 2007; Deng et al. 2014; Ismail et al. 2015; Azizi et al. 2017; Sasmaz et al. 2018; Castorina et al. 2020; Wang et al. 2022). Therefore, fluorite REE geochemistry can provide a powerful tool for discerning physic-chemical processes during hydrothermal mineralization, such as the mineralization temperature and the composition of the ore-forming fluid (e.g., Schwinn and Markl 2005; Deng et al. 2014; Sasmaz et al. 2018; Wang et al. 2022) and the ore genesis (e.g., Bau and Dulski 1995; Ismail 2015; Castorina et al. 2020).

Based on our recent research on the Baoshan Cu–Pb–Zn deposit, it is discovered that different-colored fluorites are widespread in the Baoshan Cu–Pb–Zn deposit and are usually associated in paragenesis with Pb–Zn ores or pyrite ores in the late sulfide stage. Therefore, in this contribution, we present the REE geochemistry of different colored fluorites, attempting to better elucidate the signatures of the ore-forming fluid and further understand the ore genesis of the Baoshan Cu–Pb–Zn deposit.

2 Regional geology

South China is composed of Yangtze block in the northwest and the Cathaysian block in the southwest (Chen and Jahn 1998; Li et al. 2002; Zhou et al. 2002), separated by the Qin–Hang Neoproterozoic suture, and bounded by the North China Block to the north. The Yangtze and Cathaysian blocks were welded together during the Neoproterozoic (~ 830 Ma) (e.g., Chen and Jahn 1998; Li et al. 2009; Zhao et al. 2011; Hu and Zhou 2012).

Large volumes of Mesozoic granitic rocks and related large-scale metallogeny are widespread in South China (Fig. 1; Gilder et al. 1996; Chen and Jahn 1998; Zhou et al. 2006; Li and Li 2007; Hu and Zhou 2012; Mao et al. 2013; Hu et al. 2017a, b). Most deposits are hosted by these Mesozoic granitoids and are locally controlled in the contact zones between granitoids and strata (Zhao et al. 2017). Generally speaking, W–Sn deposits are associated with granite plutons, whereas Cu–Pb–Zn deposits are associated with granodiorites (Xu et al. 1983; Hua et al. 2003; Mao et al. 2008).

By coincidence, most of the Cu–Pb–Zn deposits occur along the Qin–Hang belt and adjacent areas (Fig. 1). Based on the geological variation, three segments can be further sub-divided, i.e., the northern (northeastern), the central, and the south (southeastern) (Zhou et al. 2012). The northern (northeastern) part is characterized by the porphyry Cu–Au–Mo and epithermal Pb–Zn–Ag deposits, including the Dexing porphyry Cu–Au–Mo deposit, Yinshan porphyry Cu-epithermal Ag-Pb–Zn deposit, and Lengshuikeng porphyry Pb–Zn–Ag deposit. The central part is characterized by the skarn Pb–Zn–Cu (Mo) deposits, including the Shuikoushan hydrothermal Pb–Zn deposit, Baoshan skarn Cu–Pb–Zn deposit, and the Tongshanling skarn Cu–Pb–Zn deposit. The southern (southeastern) part is characterized by the porphyry Cu–Mo deposits, including the Yuanzhuding porphyry Cu–Mo deposit (Fig. 1; Zhou et al. 2012; Mao et al. 2013; Hu et al. 2017a, b; Yuan et al. 2018).

3 Ore deposit geology

The Baoshan Cu–Pb–Zn deposit is located in southern Hunan, South China. It is situated at the central part of the Nanling Range, including the central Cu-Mo ore block, eastern Pb–Zn–Ag ore block, northern Caishenmiao Pb–Zn–Ag ore block, and western Pb–Zn–Ag ore block (Fig. 2).

3.1 Sedimentary strata

The strata exposed in the ore district mainly consist of the Carboniferous sedimentary rocks (Fig. 2). The Devonian strata are scarce and locally occur in the eastern part. The Carboniferous series are composed of the Lower Carboniferous Menggong'ao Formation (C_1m), Shidengzi Formation (C_1sh), Ceshui Formation (C_1c), Zimenqiao Formation (C_1z), and the Middle–Lower Carboniferous Hutian Group (C_{2+3} h). The C_1m Fm. comprises sandstones interbedded with shales, and marlstones interbedded with shales. The C_1s Fm. is mainly composed of thick limestones. The C_1c Fm. consists of sandstones, siltstones, and carbonaceous shales. The C_1z Fm. consists of dolomites. The C_{2+3} h Fm. comprises the limestone in the upper part and grey–white limestone interbedded with dolomites in the lower part (Qi et al. 2018). The Pb–Zn ores in the studied deposit are mainly restricted within the C_1z Fm., C_1c Fm., and C_1s Fm. carbonate rocks (Fig. 2; Xie et al. 2015).

3.2 Structures

The magmatism and mineralization associated with the Baoshan Cu–Pb–Zn deposit were structurally controlled by complex reverse folds and faults (Fig. 2; Yin 1998). The structures in the studied area resulted from the Indosinian and Yanshanian movements. The faults mainly include early NE–NEE-trending faults (F_0, F_1, F_{21}) and late NWW-trending faults (Fig. 2).

3.3 Igneous rocks

The intrusions are widespread in the Baoshan mining district, occurring along the NWW-trending faults (Yin 1998). They are 26 exposed intrusions in total, including granodiorite-porphyry, granite-porphyry (Yin 1998), and lamprophyre (Kong et al. 2013).

Among them, granodiorite-porphyry is the most important; it intruded the Carboniferous rocks at about 156–158 Ma (Lu et al. 2006; Xie et al. 2013) with different-sized mafic microgranular enclaves (Xie et al. 2013). The phenocrysts (25–35%) consist of plagioclase, potassium feldspar, muscovite, and minor quartz, the matrices is microcrystalline and consist of feldspar, muscovite, and quartz (Xie et al. 2013). Accessory minerals mainly include apatite, zircon, rutile, allanite, sphene, thorite, and magnetite (Xie et al. 2013). These intrusions are closely associated with the Cu-polymetallic mineralization (Mi et al. 2018), with SiO_2 ranging from 61.2 wt.% to 68.8 wt.%, K_2O from 3.50 wt.% to 5.31 wt.%, the A/CNK parameter mostly in the range of 0.79–0.97 (Xie et al. 2013). They are of metaluminous to weak peraluminous rocks, belong to high-K calc-alkaline series (Xie et al. 2013), and are usually considered to be I-type granite (Wang et al. 2003; Xie et al. 2013).

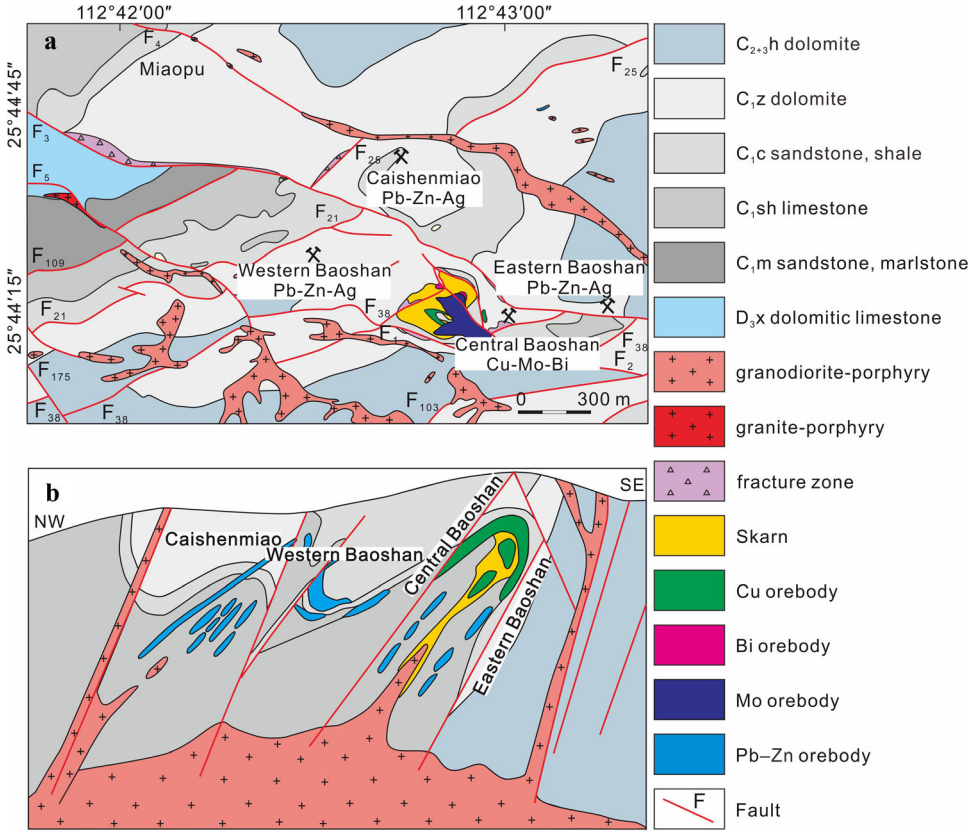

Fig. 2 **a** Simplified geological map and (**b**) cross-section map for the Baoshan Cu–Pb–Zn district, southern Hunan, South China. Modified after Yin (1998) and Xie et al. (2015)

3.4 Orebodies, ores, and mineralogy

The orebodies of the Baoshan Cu–Pb–Zn deposit are usually controlled by the Baoling reversed fold (Fig 2). The central Cu-Mo ore block is located at the top of the reversed fold, Mo–W–Bi ore block is located in the two limbs near the top of the fold and the central Cu ore block is located in the skarns of the upper of the reversed fold. The Pb–Zn–Ag ore blocks (eastern Baoshan, northern Caishenmiao, and western Baoshan) are located in the strata of the two limbs of the Baoling fold (Fig. 2).

Around the granodiorite-porphyry intrusions, the mineralization zoning can be easily observed. From core to rim, there are hydrothermal skarn Cu-Mo mineralization, mesothermal Cu–Pb–Zn mineralization, meso- and epithermal Pb–Zn–Ag mineralization, and distal Ag–Mn mineralization, respectively (Fig. 2a, Yang and Chen 1998; Tang 2005). The skarn Cu–Mo ores usually occur as veinlets-disseminated and brecciated-veins. The Pb–Zn ores, however, are massive (Xuan et al. 2017).

Ore minerals in the Baoshan Cu–Pb–Zn deposit include galena, sphalerite, pyrite, chalcopyrite, scheelite, bismuthinite, and molybdenite (Yin 1998). Gangue minerals in the deposit are dominated by fluorite, calcite, quartz, garnet, and tremolite (Mi et al. 2018).

Mineral assemblages, ore textures as well as vein crosscutting relationships indicate that the deposit can be divided into three mineralization stages, early skarn stage, retrograde and oxide stage, and late sulfide stage (Fig. 4, Qi et al. 2018). Pyrite, sphalerite, and galena are abundant in the sulfide stage, they usually occur as well-developed open-space-filling textures, such as banded (Fig. 3c), massive (Fig. 3d, e), brecciated, and porous structures (Fig. 3i). Coincidentally, sphalerite and galena are often intergrown with green fluorite (Fig. 3d, e). Pyrite, however, is frequently intergrown with violet fluorite (Fig. 3a, f–h).

4 Sampling and analytical methods

Different types of fluorite were identified by the color and paragenetic association of minerals (Fig. 3). Three green fluorite samples (BS–17, BS–19, BS–23) and four violet samples (BS–26, BS–18, BS–21, BS–22) were collected from the + 150 m mining level underground workings of the Caishenmiao ore block in the Baoshan Cu–Pb–Zn deposit for the analysis of trace elements and rare earth elements (REEs).

Mineral separates were obtained by conventional separation techniques and by subsequent handpicking under a binocular microscope (purity > 99%) and then milled to a

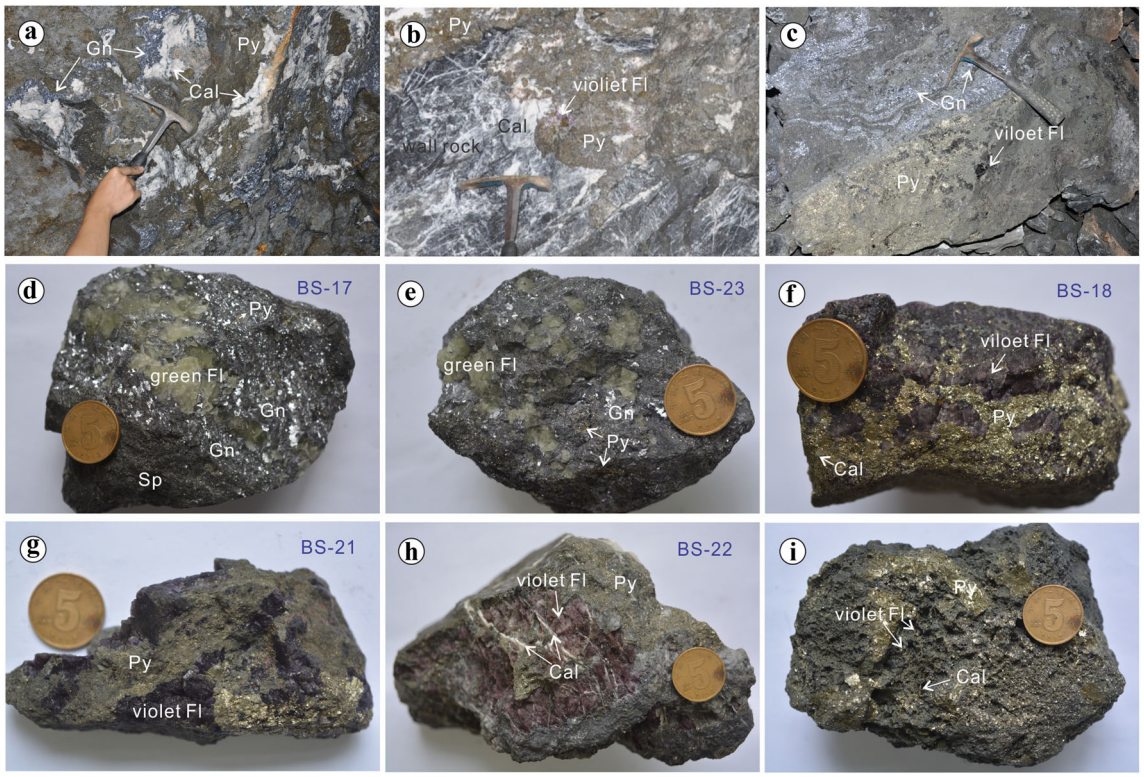

Fig. 3 Field photographs and hand specimen photographs of ores from the Baoshan Cu–Pb–Zn deposit, South China. **a** pyrite and galena in C_1sh limestone, **b** pyrite coexisting with violet fluorite in C_1sh limestone, **c** banded pyrite and galena, **d**, **e** galena coexisting with green fluorite, **f**–**h** pyrite coexisting with violet fluorite, and (**f**–**h**) porous pyrite with violet fluorite and calcite. Abbreviations: *Cal* calcite; *Fl* fluorite; *Gn* galena; *Py* pyrite

200 mesh for trace elements and REEs analyses using an inductively coupled plasma mass spectrometry (ICP-MS) with a Thermo Fisher ICP-MS X2. The analyses were performed by the Radiogenic Isotope Facility (RIF) at the University of Queensland, Australia. Powders (approximately 50–100 mg) were digested in a double-distilled HNO_3 + HF (1: 4) mixture in Teflon bombs at 185 °C for 3 days, dried, and then digested with HNO_3, and the final step was repeated. Dissolved samples were diluted to 50 mL with 2% HNO_3 and 10 ppb ^{61}Ni, 6 ppb Rh, In and Re were added to the solution as an internal standard. Instrument drift mass bias was corrected with internal spikes and external monitors. USGS standard W-2a was used as the reference standard and crossed checked with BIR-1, BHVO-2, and other reference materials. The analytical uncertainties are within 5% for most elements reported in this study.

5 Results

The analytical results are listed in Table 1 and shown in Fig. 5. Different-colored fluorite samples show different trace element and REE geochemical signatures. Green fluorites associated with Pb–Zn ores exhibit higher ΣREE concentrations, ranging from 1052 to 1680 ppm (n = 3, avg. 1381 ppm), and violet fluorites associated with pyrite vary between 148 and 350 ppm (n = 4, avg. 213 ppm) (Table 1). Both the chondrite-normalized patterns broadly share similar trends, which is characterized by marked LREE enrichment relative to heavy rare earth element (HREE) (Fig. 5), as shown by $(La/Yb)_N$ ratios for the green fluorites and violet fluorites varying from 1201–5710 (avg. 3133) and 689–1568 (avg. 1079), respectively. The Tb/La ratios of the green fluorites and violet fluorites vary in the range of 0.000344–0.000572 (avg. 0.000456) and 0.000466–0.000763 (avg. 0.000633), respectively (Table 1). Significant negative Eu anomalies are pronounced with Eu/Eu* ($Eu/Eu^* = Eu_N/\sqrt{Sm_N \times Gd_N}$) ratios, and range from 0.17 to 0.30 for green fluorites and from 0.29 to 0.48 for violet fluorites, respectively. Except for the sample BS–26 with a negative Ce anomaly ($Ce/Ce^* = Ce_N/\sqrt{La_N \times Pr_N}$ = 0.93), other samples show slightly positive Ce anomalies, and no obvious differences exist between different colored fluorites.

Green fluorites display higher La/Ho ratios (averaging 4411) than violet fluorites (2094), however, the average

Table 1 Concentrations of trace and rare earth elements for different-colored fluorite samples from the Baoshan Cu–Pb–Zn deposit (ppm)

Type	Green fluorite				Violet fluorite				
No.	BS-17	BS-19	BS-23	Avg	BS-18	BS-21	BS-22	BS-26	Avg
Li	0.304	0.342	0.201	0.282	0.772	0.589	0.303	0.582	0.562
Mg	3.50	3.65	2.61	3.25	158	25.0	31.3	134	87.1
P	3.58	5.13	4.92	4.54	13.0	7.15	7.27	9.86	9.32
Ca	499,000	503,000	510,000	504,000	503,000	497,000	501,000	504,000	501,250
Sc	0.0664	0.0712	0.0698	0.0691	0.0672	0.0744	0.0677	0.0778	0.0718
Ti	2.00	1.78	1.65	1.81	5.68	2.17	4.89	2.96	3.93
V	0.0811	0.0201	0.151	0.0841	0.394	0.216	0.135	0.360	0.276
Cr	0.129	0.101	0.0954	0.108	0.236	0.120	0.170	0.222	0.187
Mn	3.69	1.25	0.881	1.94	7.17	8.81	4.66	20.1	10.2
Fe	729	705	706	713	772	917	732	783	801
Co	0.251	0.251	0.252	0.251	0.250	0.244	0.265	0.285	0.261
Ni	4.94	4.00	3.72	4.22	3.31	3.38	4.15	7.91	4.69
Cu	1.14	1.52	0.707	1.12	22.4	15.4	15.6	2.90	14.1
Zn	2.47	1.91	3.37	2.58	3.25	2.74	2.82	2.73	2.89
Ga	7.74	5.16	6.91	6.60	0.931	1.73	0.841	0.963	1.12
Rb	0.0452	0.103	0.0500	0.0661	0.640	0.231	0.102	0.512	0.371
Sr	9.07	10.1	8.58	9.25	17.7	13.5	17.1	21.0	17.3
Pb	16.7	7.60	21.6	15.3	7.47	13.5	31.9	4.52	14.3
Bi	0.537	0.130	0.154	0.274	7.19	23.8	7.28	4.21	10.6
Th	0.143	0.0124	0.0847	0.0800	0.105	0.0349	0.0475	0.0925	0.0700
U	0.120	0.0349	0.0870	0.0806	0.806	0.575	0.315	0.418	0.529
Zr	0.0211	0.0259	0.0479	0.0316	0.426	0.0836	0.197	0.188	0.224
Mo	0.144	0.0280	0.0300	0.0673	0.120	0.0492	0.0931	0.0998	0.0905
Sn	0.347	0.0894	0.161	0.199	0.207	0.446	0.289	0.220	0.291
Sb	0.823	0.379	1.33	0.844	0.292	4.10	0.338	0.440	1.29
Cs	0.0197	0.0661	0.0145	0.033	0.0903	0.0930	0.0263	0.0478	0.0644
Ba	0.306	0.131	0.234	0.224	0.384	0.142	0.0989	1.07	0.424
Y	6.82	14.9	8.99	10.2	2.85	9.74	3.66	3.19	4.86
La	718	442	586	582	65.8	144	53.6	80.9	86.1
Ce	825	513	701	680	79.7	170	72.6	85.9	102
Pr	48.6	28.2	41.0	39.3	5.70	9.79	5.73	6.32	6.89
Nd	79.1	59.5	72.4	70.3	13.1	22.2	14.2	15.4	16.2
Sm	5.18	4.12	4.94	4.75	0.582	1.36	0.627	0.605	0.794
Eu	0.288	0.181	0.339	0.269	0.0710	0.110	0.0602	0.0610	0.0756
Gd	2.42	2.43	2.49	2.45	0.354	0.985	0.419	0.374	0.533
Tb	0.247	0.253	0.264	0.255	0.0369	0.107	0.0409	0.0377	0.0556
Dy	0.745	1.04	0.918	0.901	0.138	0.493	0.175	0.144	0.238
Ho	0.105	0.190	0.144	0.146	0.0278	0.0989	0.0333	0.0275	0.0469
Er	0.213	0.464	0.324	0.334	0.0669	0.254	0.0853	0.0688	0.119
Tm	0.0198	0.0517	0.0332	0.035	0.00815	0.0290	0.00921	0.00744	0.0135
Yb	0.0902	0.264	0.169	0.174	0.0429	0.150	0.0401	0.0370	0.0675
Lu	0.00997	0.0334	0.0198	0.021	0.00496	0.0170	0.00362	0.00394	0.00738
ΣREE	1680	1052	1410	1381	166	350	148	190	213
LREE	1676	1047	1406	1376	165	347	147	189	212
HREE	3.85	4.73	4.36	4.31	0.680	2.13	0.806	0.700	1.08
LREE/HREE	435	222	322	326	243	163	182	270	214
$(La/Yb)_N$	5710	1201	2487	3133	1100	689	959	1568	1079

Table 1 continued

Type	Green fluorite				Violet fluorite				
No.	BS-17	BS-19	BS-23	Avg	BS-18	BS-21	BS-22	BS-26	Avg
Eu/Eu*	0.25	0.17	0.30	0.24	0.48	0.29	0.36	0.39	0.30
Ce/Ce*	1.08	1.13	1.11	1.11	1.01	1.11	1.02	0.93	1.02
Tb/La	0.000344	0.000572	0.000451	0.000456	0.000561	0.000743	0.000763	0.000466	0.000633
Tb/Ca	4.95E-07	5.03E-07	5.18E-07	5.05E-07	7.34E-08	2.15E-07	8.16E-08	7.48E-08	1.11E-07
La/Ho	6838	2326	4069	4411	2367	1456	1610	2942	2094
Y/Ho	65.0	78.4	62.4	68.6	103	98.5	110	116	107

Avg, average. Eu anomaly (denoted as Eu/Eu*) calculated using the equation $Eu/Eu* = Eu_N/\sqrt{Sm_N \times Gd_N}$, $Ce/Ce* = Ce_N/\sqrt{La_N \times Pr_N}$

Y/Ho ratio for the green fluorites (68.6) is slightly lower than that of the violet fluorites (107; Table 1).

6 Discussions

6.1 REE geochemical signature and its implications

Bau and Dulski (1995) proposed that the Y–Ho fractionation is not a source-related phenomenon but depends on fluid composition and fluid migration. Due to the similar ionic radius between Y and Ho (Bau et al. 1996), they are closely coupled and behave coherently in various geological processes (Bau and Dulski 1995), and thus the Y/Ho ratio should remain constant and close to the Cl-chondritic value (28, Anders and Grevesse 1989; Bau and Dulski 1995). The green fluorites and violet fluorites from the Baoshan Cu–Pb–Zn deposit show a good linear correlation between Y and Ho with an overall R^2 value of 0.913 (R^2 = 0.998 and 0.955 respectively, Fig. 6a). Despite that the Y/Ho ratios of the studied fluorites are variable (62.4–116) and significantly higher than 28, they display highly variable La/Ho ratios at relatively constant Y/Ho ratios and thus generate a horizontal trend (recrystallization) as depicted in Fig. 6b, revealing they are cogenetic (Bau and Dulski 1995) and resulted from one thermal pulse. In addition, from the green fluorites toward the violet fluorites, they exhibit progressively increasing or decreasing REE trends in Fig. 7, which also support the above deduction.

However, the Y/Ho ratios of the studied fluorites (62.4–116) well overlapped the Y/Ho ratios of hydrothermal fluorites (Fig. 8), partly overlapped the range of seawater and higher than the Baoshan granodiorite-porphyry (18.0–30.7). Moreover, they are similar to the violet fluorites from the Au ores from the Shuikoushan Pb–Zn–Au deposit, whose Y/Ho ratios range from 60.8 to 125. Therefore, it seems to suggest that the fluorites from the Baoshan Cu–Pb–Zn deposit were formed by the interaction of the local granodiorite-porphyry magmatic hydrothermal fluid with a non-magmatic fluid, which is characterized by higher Y/Ho ratios than the fluorites.

REE fractionation in fluids is related to either preferential adsorption of REE in minerals or preferential complexation of REE with different ligands (Bau 1991; Bau and Dulski 1995; Deng et al. 2014). REE can be preferentially adsorbed in some hydrothermal minerals such as calcite (Ehya 2012; Deng et al. 2014), thus, the REE abundance in hydrothermal fluids may depend on the crystallization sequence of REE-bearing minerals, regardless of the REE source (e.g. Castorina et al. 2008; Ehya 2012; Deng et al. 2014). At the Baoshan deposit, however, the only carbonate mineral (calcite) was generally deposited later than fluorite (Fig. 3h), and we can rule out the REE preferential adsorption effect on the REE abundance in the studied fluorites.

All fluorite samples from the Baoshan deposit exhibit similar chondrite-normalized patterns with pronounced LREE enrichment (Table 1; Fig. 5), and elevated $(La/Yb)_N$ values ranging from 689 to 5710 (Table 1). Möller et al. (1976) indicated that LREE is preferentially concentrated in the early-crystallized fluorites and thus displays elevated $(La/Yb)_N$ ratios. Therefore, it can be suggested that the studied fluorites probably precipitated at the early hydrothermal sulfide stage, and Pb–Zn ores crystallized earlier than pyrite ores (Ismail et al. 2015). This agrees well with the geological relationship of the minerals (Figs. 3 and 4). LREE-enrichment is also a discriminative characteristic for those fluorites formed under high-temperature (T) and low-pH (Ehya 2012; Deng et al. 2014). This can be further supported by the conclusion that the ore-forming fluid from the sulfide stage for the Baoshan deposit is characterized by moderate to high temperatures (Xuan et al. 2017) and low pH value (see 6.2).

Generally, the stabilities of REE–F complexes have been known to increase from La to Lu (Möller et al. 1976; Wood 1990; Hass et al. 1995). Thus, the early-crystallized fluorites are rich in LREE and poor in HREE, the late

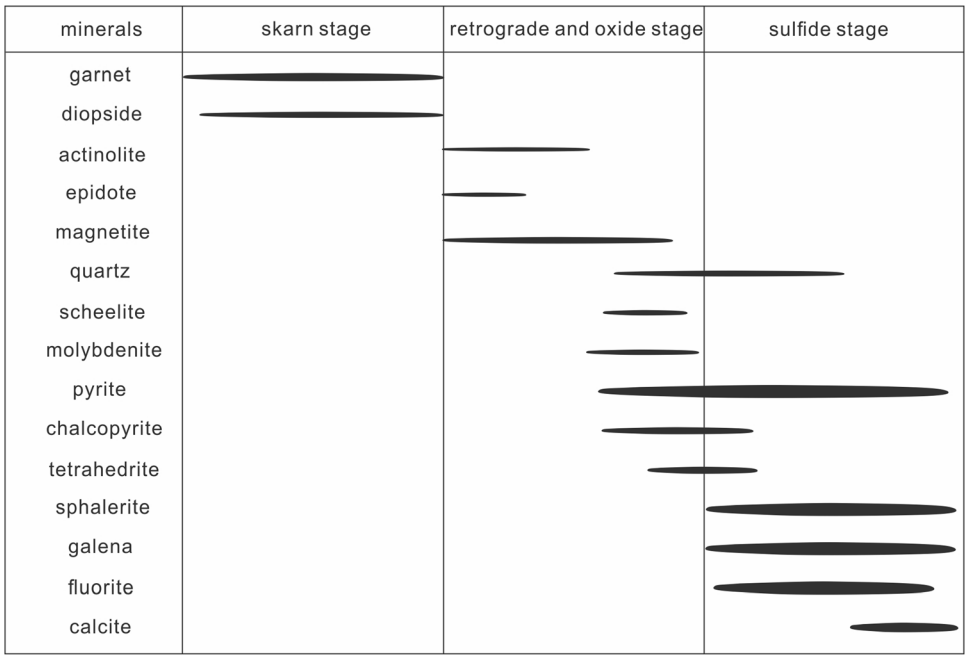

Fig. 4 Mineral sequence and ore-forming stages of the Baoshan Cu–Pb–Zn deposit. Modified after Qi et al. (2018)

crystallized fluorites, however, are rich in HREE and poor in LREE. Moreover, La and Tb are intensely fractionated in fluorites, thus the early-crystallized fluorites display lower Tb/La ratios, while the late-crystallized fluorites display higher Tb/La ratios (Constantopoulos 1988; Sasmaz and Yavuz 2007). Consequently, the REE patterns and the Tb/La ratios can help to define the stages of the mineralization (Möller et al. 1976; Peng et al. 2002).

The studied different colored fluorites in the Baoshan Cu–Pb–Zn deposit exhibit similar REE patterns and proximate Tb/La ratios, which suggest that they may have been deposited crystallized in a short time (Constantopoulos 1988). However, green fluorites exhibit slightly lower

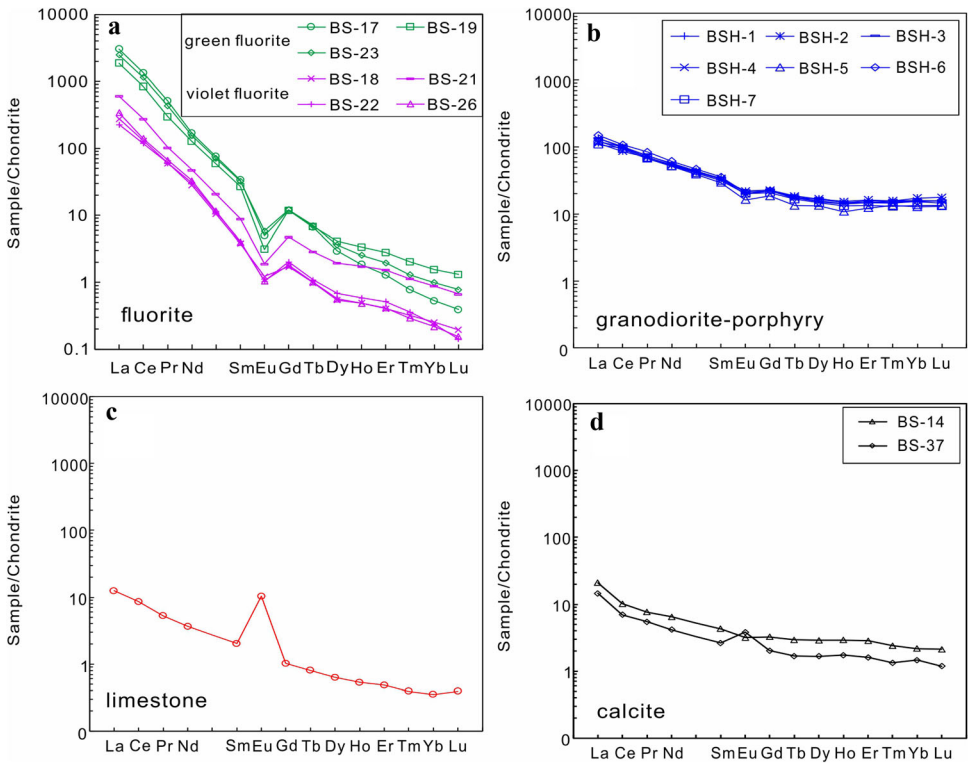

Fig. 5 Chondrite-normalized REE patterns for fluorite (**a**), granodiorite-porphyry (**b**), limestone (**c**), and calcite (**d**) samples from the Baoshan Cu–Pb–Zn deposit. The reference data of chondrite are cited from Sun and McDonough (1989). Data of the granodiorite-porphyry are from Wang et al. (2003). Data of limestone and calcite are from Yao et al. (2006)

mean Tb/La ratios than the violet fluorites (Table 1) also suggests that the green fluorites (Pb–Zn ores) precipitated relatively earlier than the violet fluorites (pyrite ores).

In addition, the similar REE patterns for the studied fluorites also indicate that they were precipitated in an open system (Möller 1991), which might continuously supply ore-forming solution to the depositional site (Peng et al. 2002). This could be further supported by the above-discussed well-developed open-space-filling textures in the Baoshan deposit (Fig. 3).

Coincidentally, the trace element and REE concentrations regularly vary with the color of fluorite. From the green fluorites to the violet fluorites, they display a decreasing tendency in concentrations for all the trace elements except REE, Ga, Pb, and Th, and the latter exhibit an opposite trend (Table 1; Figs. 5, 7). Thus, we can attribute the different colors of fluorites in the Baoshan Cu–Pb–Zn deposit to the trace element concentrations in the fluorites.

Schwinn and Markl (2005) showed that the ΣREE concentration in hydrothermal fluids is controlled by the pH and bulk chemical composition of solutions. It is assumed that REE concentration in hydrothermal solutions increases with the decreasing pH (Michard 1989). Nonetheless, green fluorites display significantly higher ΣREE concentrations than the violet fluorites (Table 1), probably reflecting green fluorites precipitated under a lower pH condition (more acidic) than violet fluorites as Michard (1989) proposed.

The Eu/Eu* ratio is a useful indicator of the physicochemical features of fluids, including temperature, pH (Bau 1991; Castorina 2008), and fO_2 (Bau and Möller 1992; Castorina 2008). In general, the thermochemical reduction of Eu^{3+} to Eu^{2+} can happen at $T > 200$ °C (Schiwinn and Markl 2005) or 250 °C (Bau 1991). In addition, the fO_2 value for the reduction of Eu^{3+} increases with the increasing temperature (Bau 1991). The larger radius of Eu^{2+} prevents it from substituting for Ca^{2+} in fluorite (Constantopoulos 1988), triggering the decoupling of the Eu from the trivalent REE neighbors, and thus resulting in the negative Eu anomaly for fluorite (Bau 1991; Bau and Möller 1992; Castorina 2008). Alternatively, Eu anomaly in the fluorite can be also an indicator of the parental fluid (Schiwinn and Markl 2005; Castorina 2008), since fluorites can inherit the REE characteristics from the parental fluid.

All the fluorites from the Baoshan deposit display pronounced negative Eu anomalies (Fig. 5a), with average Eu/Eu* value increasing from 0.24 for the green fluorite to 0.30 for the violet fluorite (Table 1). This suggests the fluorites crystallized either at $T > 200$ °C from a fluid with or without Eu anomaly or at $T < 200$ °C from a fluid with a negative Eu anomaly (Schiwinn and Markl 2005; Castorina 2008). As depicted in Fig. 4b, the Baoshan granodiorite-porphyry, from which the fluid was probably originated (Xuan et al. 2017; Ding et al. 2016; Zhang et al. 2018), also displays obvious negative Eu anomaly. In addition, fluid inclusion homogenization temperatures for the sulfide stage are clustered in the range of 190–240 °C (Xuan et al. 2017), mostly above 200 °C. Therefore, this indicates the fluorites precipitated from fluids with high temperature, low and increasing fO_2 values.

The Ce/Ce* ratio can be another indicator for the physicochemical features of hydrothermal fluids (Deng et al. 2014). At the condition of high fO_2, Ce^{3+} is prone to be oxidized to immobile Ce^{4+}, which is apt to be hydrolyzed and absorbed by the oxides or hydroxides and thus separated from the fluid, consequently resulting in a negative Ce anomaly of the fluid and its precipitant (Möller and Morteani 1983). All but one of the fluorites show slightly positive Ce anomalies, with a range of 1.08–1.13 (avg. 1.11) for green fluorites and 0.93–1.11 (avg. 1.02) for violet fluorites, indicating that there is low fO_2 at the source of the hydrothermal fluids and the resultant reduction of Ce^{4+} and immobilization of Ce^{3+} (Constantopoulos 1988). This is consistent with the negative Eu anomalies in fluorites. In addition, the weakly positive Ce anomalies may also be inherited from the parent fluid (Castorina 2008; Ehya 2012), which probably be the Baoshan granodiorite-porphyry with weakly positive Ce anomalies (Fig. 5b; Table 1).

6.2 Sources of REE and fluid

As depicted in Fig. 3, the granodiorite-porphyry rocks and the fluorites exhibit similar chondrite-normalized patterns with pronounced LREE enrichment and negative Eu anomalies. In addition, as shown in H–O isotope composition (Xuan et al. 2017), S and Pb isotope composition (e.g. Yao et al. 2006; Zhu et al. 2012; Xie et al. 2015; Ding et al. 2016; Zhang et al. 2018), C–O isotope composition (Xie et al. 2015) and zircon U–Pb age of 156–158 Ma for the granodiorite-porphyry (Lu et al. 2006; Xie et al. 2013), it is indicated that the LREE-enriched fluid could be sourced from the granodiorite-porphyry with involvement of the Carboniferous carbonates.

However, the fluorites, especially the green fluorites, display significantly higher ΣREE concentrations (1052–1680 ppm) than the granodiorite-porphyry (135–161 ppm) and the limestone (12 ppm) (Fig. 5; Tables 1 and 2). In addition, the limestone displays remarkably Eu anomalies which are different from the fluorites (Fig. 4). Thus, only the magma fluid and the Carboniferous carbonates are incapable of providing sufficient REE for the fluorites. Therefore, we proposed that there is another important undetected non-magmatic source to provide sufficient REE for the fluorites.

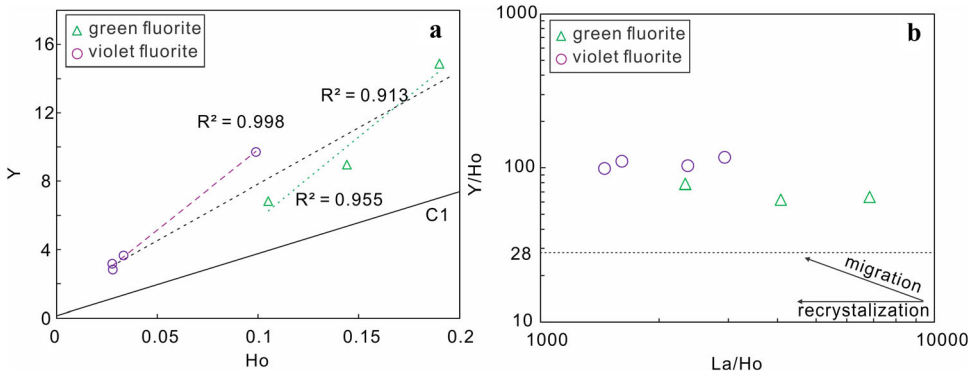

Fig. 6 Diagrams of (**a**) Y versus Ho and (**b**) Y/Ho versus La/Ho ratios for the fluorites from the Baoshan Cu–Pb–Zn deposit

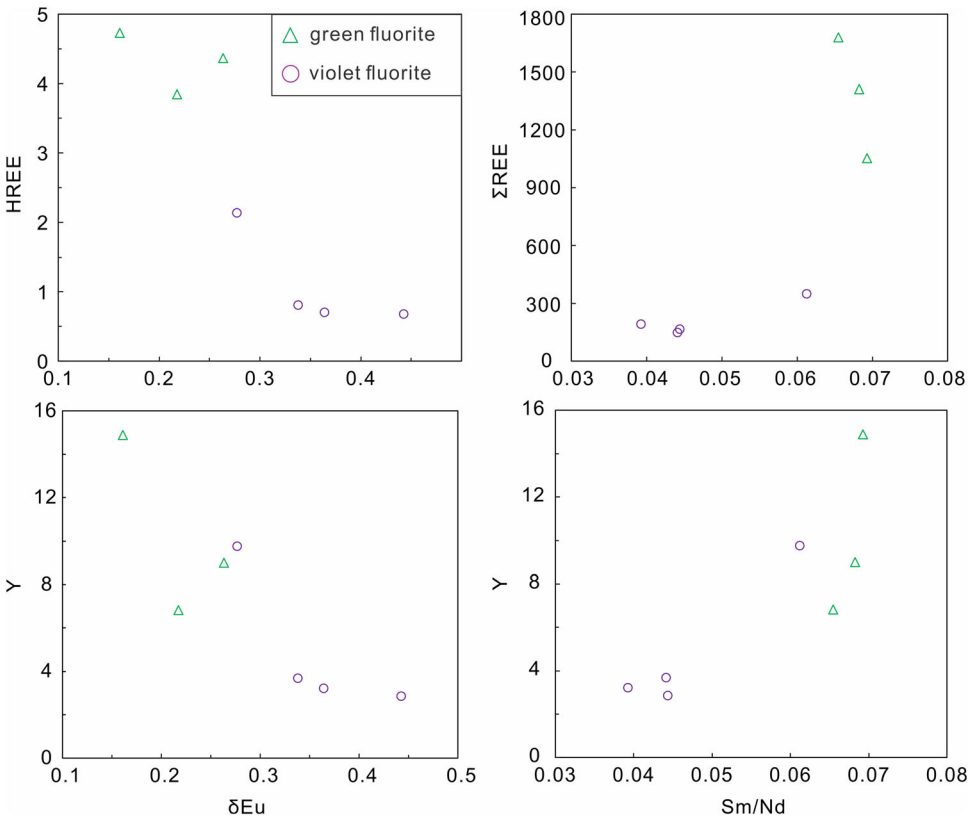

Fig. 7 Variation diagram of REE in fluorites from the Baoshan Cu–Pb–Zn deposit

6.3 Constraints on the deposition mechanism for fluorite

Richardson and Holland (1979) suggested three mechanisms are responsible for fluorite deposition: changes in temperature and/or pressure, fluid mixing, and wall rocks reaction.

Due to the fluid inclusion homogenization temperatures for the sulfide stage are clustered (190–240 °C) (Xuan et al. 2017), thus temperature changes only could not lead to the precipitation of fluorites. In addition, boiling inclusions in fluorites were not widely observed (Xuan et al. 2017). Thus, decreasing pressure also could not play an important role in the deposition of fluorites. Field geological relationship reveals that the fluorites mainly coexist with the ores and exhibit clear contact boundary with the wall rocks (Fig. 3). Therefore, the wall-rock reaction can be ruled out as a major cause of fluorite deposition.

As discussed above, the fluorites were precipitated in an open system (Fig. 3), suggesting that external fluid can be progressively supplied to the precipitation site. Coincidentally, H and O isotope composition provide convincing

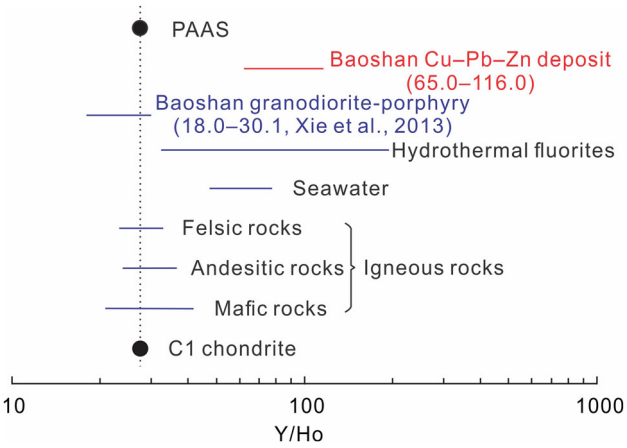

Fig. 8 Comparison of the Y/Ho ratios from the Baoshan Cu–Pb–Zn deposit with the ratios from other kinds of geological bodies (Bau and Dulski, 1995)

evidence of a significant input of meteoric water into the magmatic fluid (Xuan et al. 2017). Alternatively, the relatively wide variation in homogenization temperatures of 156.7–323.1 °C, clustering in the range of 190–240 °C and decreases with the decreasing salinities (3.71–19.84 %; Xuan et al. 2017), also provide reliable evidence for the fluid mixing. As mentioned above, a non-magmatic source is involved in fluorite precipitation.

To sum up, fluid mixing between magma fluid and an undetected non-magmatic fluid probably is the most appealing mechanism for fluorite deposition in the Baoshan deposit. The deposition time and the physical-chemistry condition (ie. increasing pH and fO_2 values) contributed to the difference of REE characteristics between the green fluorites and violet fluorites.

7 Conclusions

The ΣREE concentrations in the green fluorites and violet fluorites are extremely high with similar LREE-enrichment, pronounced negative Eu anomalies, and weakly positive Ce anomalies. The fluorites were probably deposited under middle-high T and low-pH conditions.

The Y/Ho ratios suggest that the green fluorites and the violet fluorites were cogenetic. The similar Tb/La ratios for the studied fluorites reveal that both green fluorites and violet fluorites formed in a short time at an early stage sulfide mineralization stage. From the green fluorites to violet fluorites, ΣREE concentrations, $(La/Yb)_N$ ratios, Tb/La ratios, and Ce/Ce* ratio decreases, but the Eu/Eu* ratio increases, suggesting that the green fluorites precipitated earlier and the fluid became less reducing, less acidic, and lower in temperature.

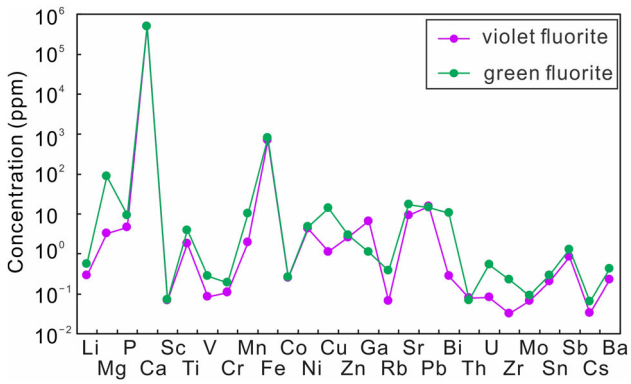

Fig. 9 Variations of the trace elements for green and violet fluorites for the Baoshan Cu–Pb–Zn deposit

Table 2 Concentrations of rare earth and trace elements for magmatic rocks, sedimentary rocks and calcite from the Baoshan Cu–Pb–Zn deposit (ppm)

Type	Granodiorite-porphyry							Limestone	Calcite	
No.	BSH-1	BSH-2	BSH-3	BSH-4	BSH-5	BSH-6	BSH-7		BS-14	BS-37
La	32.3	27.1	32.1	28.7	29.4	35.6	25.8	2.96	4.99	3.45
Ce	60.8	53	62.5	61.1	57	66.1	58.5	5.28	6.25	4.26
Pr	6.71	6.72	7.03	7.05	6.37	8.01	6.65	0.50	0.73	0.52
Nd	25.2	24.8	26.6	25.8	24.1	28.6	24.3	1.71	3.03	1.95
Sm	5.27	5.11	5.12	5.19	4.5	5.46	4.83	0.31	0.66	0.40
Eu	1.22	1.28	1.15	1.15	0.94	1.22	1.17	0.60	0.18	0.22
Gd	4.56	4.67	4.61	4.54	3.81	4.54	4.27	0.21	0.67	0.42
Tb	0.68	0.69	0.63	0.66	0.5	0.65	0.62	0.03	0.11	0.06
Dy	4.18	4.26	4.34	3.98	3.35	3.83	3.72	0.16	0.74	0.42
Ho	0.85	0.87	0.83	0.81	0.61	0.79	0.74	0.03	0.17	0.10
Er	2.44	2.68	2.57	2.46	2.03	2.42	2.23	0.08	0.47	0.27
Tm	0.4	0.4	0.4	0.38	0.34	0.37	0.33	0.01	0.06	0.03
Yb	2.58	2.94	2.72	2.64	2.16	2.62	2.28	0.06	0.37	0.25
Lu	0.37	0.45	0.4	0.4	0.33	0.4	0.34	0.01	0.05	0.03
Y	24.4	23.8	24.4	22.9	18.7	21.8	13.3	0.74	4.84	2.69
Ca	33,327	26,877	26,375	20,355	16,699	25,587	42,716			
ΣREE	148	135	151	145	135	161	136	12.0	18.5	12.4
LREE	132	118	135	129	122	145	121	11.4	15.8	10.8
HREE	16.1	17.0	16.5	15.9	13.1	15.6	14.5	0.59	2.6	1.6
LREE/HREE	8.19	6.96	8.15	8.13	9.32	9.28	8.3	19.3	6.0	6.9
La_N/Yb_N	8.99	6.61	8.47	7.80	9.76	9.75	8.12	35.4	9.67	9.97
Eu/Eu*	0.76	0.80	0.72	0.72	0.69	0.75	0.79	7.19	0.85	1.66
Ce/Ce*	1.01	0.96	1.02	1.05	1.02	0.96	1.10	1.06	0.80	0.78
Y/Ho	28.7	27.4	29.4	28.3	30.7	27.6	18.0	24.7	29.3	27.4
Tb/Ca	0.0000204	0.0000257	0.0000239	0.0000324	0.0000299	0.0000254	0.0000145			
Tb/La	0.02	0.03	0.02	0.02	0.02	0.02	0.02			

Avg average. Eu anomaly (denoted as Eu/Eu*) calculated using the equation$Eu/Eu* = Eu_N/\sqrt{Sm_N \times Gd_N}$, $Ce/Ce* = Ce_N/\sqrt{La_N \times Pr_N}$. Data of granodiorite-porphyry are from Wang et al. (2003), data of limestone and calcite are from Yao et al. (2006)

The REE in the fluorite is partly derived from the Baoshan granodiorite-porphyry and an undetected non-magmatic source. The most plausible mechanism of the studied fluorites seems to be fluid mixing.

Acknowledgements This research was financially supported by the National Natural Science Foundation of China (No. 42102079), the Natural Science Foundation of Sichuan Province (No. 22NSFSC2765), State Key Laboratory of Ore Deposit Geochemistry Key Laboratory Open Project Fund (No. 201804), and the Southwest University of Science and Technology Doctoral Fund (No. 16zx7132). We thank the geologists of the Baoshan Nonferrous-metal Corporation for their help during our field investigations and Dr. Nengping Shen for his help with the analysis assistance.

Declarations

Conflict of interest The authors declare that they have no known competing financial interests or personal relationships that could have appeared to influence the work reported in this paper.

References

Anders E, Grevesse N (1989) Abundances of the elements: meteoritic and solar. Geochim Cosmochim Acta 53(1):197–214. https://doi.org/10.1016/0016-7037(89)90286-X

Azizi MR, Abedenini A, Alipour S, Niroomand S, Sasmaz A, Talaei B (2017) Rare earth element geochemistry and tetrad effect in fluorites: a case study from the Qahr-Abad deposit. Iran N Jb Palont Abh 283(3):255–273. https://doi.org/10.1127/njgpa/2017/0639

Bao T, Ye L, Yang YL, Li ZL (2014) Characteristics of sulfur isotope geochemistry of Baoshan Cu-Mo–Pb-Zn-Ag polymetallic deposit, Hunan Province and its geological significance. Acta Miner Sinica 34(2):261–266 **(in Chinese with English abstract)**

Bau M (1991) Rare-earth element mobility during hydrothermal and metamorphic fluid-rock interaction and the significance of the oxidation state of europium. Chem Geol 93(3):219–230. https://doi.org/10.1016/0009-2541(91)90115-8

Bau M (1996) Controls on the fractionation of isovalent trace elements in magmatic and aqueous systems: evidence from Y/Ho, Zr/Hf, and lanthanide tetrad effect. Contrib Miner Petr 123(3):323–333

Bau M, Dulski P (1995) Comparative study of Yttrium and rare-earth element behaviours in fluorine-rich hydrothermal fluids. Contrib Miner Petr 119(2–3):213–223

Bau M, Möller P (1992) Rare earth element fractionation in metamorphogenic hydrothermal calcite, magnesite and siderite. Miner Petrol 45(3–4):231–246

Castorina F, Masi U, Gorello I (2020) Rare earth element and Sr-Nd isotopic evidence for the origin of fluorite from the Silius vein deposit (southeastern Sardinia, Italy). J Geochem Explor 215:106535. https://doi.org/10.1016/j.gexplo.2020.106535

Castorina F, Masi U, Padalino G, Palomba M (2008). Trace-element and Sr–Nd isotopic evidence for the origin of the Sardinian fluorite mineralization (Italy). Appl Geochem 23(10):2906–2921. https://doi.org/10.1016/j.apgeochem.2008.04.005

Chen JF, Jahn BM (1998) Crustal evolution of Southeastern China, Nd and Sr isotopic evidence. Tectonophysics 284:101–133. https://doi.org/10.1016/S0040-1951(97)00186-8

Constantopoulos J (1988) Fluid inclusions and rare earth element geochemistry of fluorite from South-Central Idaho. Econ Geol 83(3):626–636. https://doi.org/10.2113/gsecongeo.83.3.626

Deng XH, Chen YJ, Yao JM, Bagas L, Tang HS (2014) Fluorite REE–Y (REY) geochemistry of the Ca. 850 Ma Tumen molybdenite–fluorite deposit, Eastern Qinling, China: constraints on ore genesis. Ore Geol Rev 63:532–543. https://doi.org/10.1016/j.oregeorev.2014.02.009

Ding T, Ma DS, Lu JJ, Zhang RQ, Xie YC (2016) Sulfur and lead isotopic compositions of granitoids and fluid inclusions in Baoshan deposit, Hunan Province. Miner Depos 35(04):663–676 **(in Chinese with English abstract)**

Ehya F (2012) Variation of mineralizing fluids and fractionation of REE during the emplacement of the vein-type fluorite deposit at Bozijan, Markazi Province. Iran J Geochem Explor 112:93–106. https://doi.org/10.1016/j.gexplo.2011.08.005

Elzinga EJ, Reeder RJ, Withers SH, Peale RE, Mason RA, Beck KM, Hess WP (2002) EXAFS study of rare-earth element coordination in calcite. Geochim Cosmochim Acta 66(16):2885. https://doi.org/10.1016/s0016-7037(02)00888-8

Gilder SA, Gill J, Coe RS, Zhao XX, Liu ZW, Wang GX, Yuan KR, Liu WL, Kuang GD, Wu HR (1996) Isotopic and paleomagnetic constraints on the Mesozoic tectonic evolution of south China. J Geophys Res Solid Earth 101:16137–16154. https://doi.org/10.1029/96JB00662

Haas Johnson R, Shock Everett L, Sassani David C (1995) Rare earth elements in hydrothermal systems: estimates of standard partial molal thermodynamic properties of aqueous complexes of the rare earth elements at high pressures and temperatures. Geochim Cosmochim Acta 59:4329–4350. https://doi.org/10.1016/0016-7037(95)00314-P

Hu RZ, Zhou MF (2012) Multiple Mesozoic mineralization events in South China—an introduction to the thematic issue. Miner Depos 47(6):579–588. https://doi.org/10.1007/s00126-012-0431-6

Hu RZ, Chen WT, Xu DR, Zhou MF (2017a) Reviews and new metallogenic models of mineral deposits in South China: an introduction. J Asian Earth Sci 137:1–8. https://doi.org/10.1016/j.jseaes.2017.02.035

Hu RZ, Fu SL, Huang Y, Zhou MF, Fu SH, Zhao CH, Wang YJ, Bi XW, Xiao JF (2017b) The giant South China Mesozoic low-temperature, metallogenic domain: reviews and a new geodynamic model. J Asian Earth Sci 137:9–34. https://doi.org/10.1016/j.jseaes.2016.10.016

Hua RM, Mao JW (1999) A preliminary discussion on the mesozoic metallogenic explosion in East China. Miner Depos 18(4):300–308 **(in Chinese with English abstract)**

Hua RM, Chen PR, Zhang WL, Liu XD, Lu JJ, Lin JF, Yao JM, Qi HW, Zhang ZS, Gu SY (2003) Metallogenic systems related to mesozoic and cenozoic granitoids in South China. Sci China Ser D 46:816–829

Ismail I, Baioumy H, Ouyang H, Mossa H, Aly HF (2015) Origin of fluorite mineralizations in the Nuba Mountains, Sudan and their rare earth element geochemistry. J Afr Earth Sci 112:276–286. https://doi.org/10.1016/j.jafrearsci.2015.09.016

Kong H, Quan TJ, Zhong JL, Chen ZF, Wang G, Guo BY, Zhao ZQ (2013) Geochemical characteristics of lamprophyre and its geological significance in Baoshan deposit, Hunan province, China. Chin J Nonferr Metal 23(09):2671–2682 **(in Chinese with English abstract)**

Li ZX, Li XH (2007) Formation of the 1300-km-wide intracontinental orogen and postorogenic magmatic province in Mesozoic South China: a flat-slab subduction model. Geology 35(2):179–182

Li ZX, Li XH, Zhou HW, Kinny PD (2002) Grenvillian continental collision in South China: new SHIMP U-Pb zircon results and implications for the configuration of Rodinia. Geology 30(2):163–166

Li XH, Li WX, Li ZX, Lo CH, Wang J, Ye MF, Yang YH (2009) Amalgamation between the Yangtze and Cathaysia Blocks in South China: constraints from SHRIMP U-Pb zircon ages, geochemistry and Nd–Hf isotopes of the Shuangxiwu volcanic rocks. Precambrian Res 174(1):117–128. https://doi.org/10.1016/j.precamres.2009.07.004

Li XF, Hu RZ, Hua RM, Ma DS, Wu LY, Qi YQ, Peng JT (2013) The Mesozoic syntexis type granite-related Cu-Pb-Zn mineralization in South China. Acta Petrol Sinica 29(12):4037–4050 **(in Chinese with English abstract)**

Lu YF, Ma LY, Qu WJ, Mei YP, Chen XQ (2006) U-Pb and Re–Os isotope geochronology of Baoshan Cu-Mo polymetallic ore deposit in Hunan province. Acta Petrol Sinica 22(10):2483–2492 **(in Chinese with English abstract)**

Mao JW, Xie GQ, Guo CL, Yuan SD, Cheng YB, Chen YC (2008) Spatial-temporal distribution of Mesozoic ore deposits in South China and their metallogenic settings. Geol J China U 14:510–526 **(in Chinese with English abstract)**

Mao JW, Chen MH, Yuan SD, Guo CL (2011) Geological characteristics of the Qin-Hang (or Shihang) metallotenic belt in South China and spatial-temporal distribution regularity of mineral deposits. Acta Geol Sini 85(5):636–658 **(in Chinese with English abstract)**

Mao JW, Cheng YB, Chen MH, Franco P (2013) Major types and time-space distribution of Mesozoic ore deposits in South China and their geodynamic settings. Miner Deposita 48:267–294. https://doi.org/10.1007/s00126-012-0446-z

Maruyama S, Isozaki Y, Kimura G, Terabayashi M (1997) Paleogeographic maps of the Japanese islands: plate tectonic synthesis from 750 Ma to the present. Island Arc 6(1):121–142. https://doi.org/10.1111/j.1440-1738.1997.tb00043.x

Mi JR, Yuan SD, Xuan YS, Zhang DL (2018) Zircon U-Pb ages Hf isotope and trace element characteristics of the granodiorite porphyry from the Baoshan-Dafang ore district, Hunan: implications for regional metallogeny. Acta Petrol Sinica 34(9):2548–2564 **(in Chinese with English abstract)**

Michard A (1989) Rare earth element systematics in hydrothermal fluids. Geochim Cosmochim Acta 53(3):745–750. https://doi.org/10.1016/0016-7037(89)90017-3

Möller P, Parekh P, Schneider HJ (1976) The application of Tb/Ca–Tb/La abundance ratios to problems of fluorspar genesis. Miner Deposita 11(1):111–116

Möller P, Morteani G (1983) On the geochemical fractionation of rare earth elements during the formation of Ca-minerals and its application to problems of the genesis of ore deposits. In: The significance of trace elements in solving petrogenetic problems and controversies. Theophrastus Athens: 747–791

Möller P (1991) REE fractionation in hydrothermal fluorite and calcite. In: Pagel M, Leroy JL (ed) Source, transport and deposition of metals. 25th SGA Anniversary Meeting: Rotterdam

Peng JT, Hu RZ, Qi L (2002) REE geochemistry of fluorite from the Qinglong antimony deposit and its geological implications. Chin J Geol 37(3):277–287 **(in Chinese with English abstract)**

Qi FY, Zhang Z, Zhu XY, Li YS, Zhen SM, Gong FY, Gong XD (2018) Mineral chacterisics and geological significance of the Baoshan Cu-Pb-Zn polymetallic deposit in Hunan Province. J Jilin Univ (Earth Sci Ed) 48(03):754–768 **(in Chinese with English abstract)**

Richardson CK, Holland HD (1979) Fluorite deposition in hydrothermal systems. Geochim Cosmochim Acta 43(8):1327–1335. https://doi.org/10.1016/0016-7037(79)90122-4

Sasmaz A, Yavuz F (2007) REE geochemistry and fluid-inclusion studies of fluorite deposits from the Yaylagözü area(Yildizeli-Sivas) in Central Turkey. N Jb Miner Abh 183(2):215–226

Sasmaz A, Yavuz F, Sagiroglu A, Akgul B (2005a) Geochemical patterns of the Akdagmadeni (Yozgat, Central Turkey) fluorite deposits and implications. J Asian Earth Sci 24(4):469–479. https://doi.org/10.1016/j.jseaes.2004.01.003

Sasmaz A, Önal A, Sagiroglu A, Önal M (2005b) Origin and nature of the mineralizing fluids of thrust zone fluorites in Çelikhan (Adiyaman, Eastern Turkey): a geochemical approach. Geochem J 39(2):131–139. https://doi.org/10.2343/geochemj.39.131

Sasmaz A, Kryuchenko N, Zhovinsky E, Suyarko V, Konakci N, Akgul B (2018) Major, trace and rare earth element (REE) geochemistry of different colored fluorites in the Bobrynets Region, Ukraine. Ore Geol Rev 102:338–350. https://doi.org/10.1016/j.oregeorev.2018.09.014

Schneider HJ, Möller P, Parekh PP (1975) Rare earth elements distribution in fluorites and carbonate sediments of the East-Alpine Mid-Triassic sequences in the Nördliche Kalkalpen. Miner Deposita 10(4):330–344

Schwinn G, Markl G (2005) REE systematics in hydrothermal fluorite. Chem Geol 216(3):225–248

Sun SS, McDonough WF (1989) Chemical and isotopic systematics of oceanic basalts: implications for mantle composition and processes. Geol Soc Lond Spec Publ 42(1):313–345. https://doi.org/10.1144/GSL.SP.1989.042.01.19

Tang CY (2005) Structural controlling characteristics of mineralization in Baoshan polymetallic ore field, Hunan province. Miner Resour Geol 1(19):43–47 **(in Chinese with English abstract)**

Wang YJ, Fan WM, Guo F (2003) Geochemistry of early mesozoic potassium-rich diorites-granodiorites in southeastern Hunan Province, South China: petrogenesis and tectonic implications. Geochem J 37:427–448. https://doi.org/10.2343/geochemj.37.427

Wang L, Tang L, Zhang ST, Santosh M, Song KR, Sheng YM, Feng JY (2022) Genesis of a Ag-Pb-Zn-F system: insights from *in-situ* sulfur isotope and trace elements of pyrite, and rare earth elements of fluorite in the Baiyine'lebu deposit, Inner Mongolia, China. Ore Geol Rev 141:104667. https://doi.org/10.1016/j.oregeorev.2021.104667

Wood Scott A (1990) The aqueous geochemistry of the rare-earth elements and yttrium: 2. Theoretical predictions of speciation in hydrothermal solutions to 350°C at saturation water vapor pressure. Chem Geol 88:99–125. https://doi.org/10.1016/0009-2541(90)90106-H

Xie YC, Lu JJ, Ma DS, Zhang RQ, Gao JF, Yao Y (2013) Origin of granodiorite porphyry and mafic microgranular enclave in the Baoshan Pb-Zn polymetallic deposit, southern Hunan Province: zircon U-Pb chronological, geochemical and Sr–Nd–Hf isotopic constraints. Acta Petrol Sin 29(12):4186–4214 **(in Chinese with English abstract)**

Xie YC, Lu JJ, Yang P, Ma DS, Xu ZW, Zhang RQ, Cai Y, Ding T (2015) S, Pb, C and O isotopic characteristics and sources of metallogenic materials of Baoshan Pb-Zn deposit, southern Hunan Province. Miner Depos 34(02):333–351 **(in Chinese with English abstract)**

Xu KQ, Hu SX, Sun MZ, Zhang JR, Ye J (1983) On the genetic series of granites, as exemplified by the Mesozoic granites of South China. Acta Geol Sin 57:97–106 **(in Chinese with English abstract)**

Xuan YS, Yuan SD, Mi JR, Zhao PL, Yuan YB, Zhang DL (2017) Preliminary studies on the fluid inclusions and H-O isotopic geochemistry of the Baoshan copper polymetallic deposit Hunan Province. Acta Petrol Sinica 33(3):873–886 **(in Chinese with English abstract)**

Yao JM, Hua RM, Lin JF (2006) REE, Pb-S isotope geochemistry, and Rb-Sr isochron age of pyrites in the Baoshan deposit, South Hunan Province, China. Acta Geol Sinica 80(7):1045–1054 **(in Chinese with English abstract)**

Yin JP (1998) Metallognic tectonics analysis about Baoshan Pb-Zn-Ag polymetallic deposit, Hunan, China. Geotectonica Metall S1:57–61 **(in Chinese with English abstract)**

Yuan SD, Mao JW, Zhao PL, Yuan YB (2018) Geochronology and petrogenesis of the Qibaoshan Cu-polymetallic deposit, Northeastern Hunan Province: implications for the metal source and metallogenic evolution of the intracontinental Qinhang Cu-polymetallic Belt, South China. Lithos 302–303:519–534. https://doi.org/10.1016/j.lithos.2018.01.017

Zhang Y, Luo JB, Kong H, Quan TJ, Xi XS (2018) Geochemical characteristics and geological significance of sulfur isotopes in the Baoshan Pb-Zn-Ag deposit, southern Hunan Province. Geol Explor 54(1):82–89 **(in Chinese with English abstract)**

Zhao JH, Zhou MF, Yan DP, Zheng JP, Li JW (2011) Reappraisal of the ages of Neoproterozoic strata in South China: no connection with the Grenvillian Orogeny. Geology 39(4):299–302. https://doi.org/10.1130/G31701.1

Zhao PL, Yuan SD, Mao JW, Santosh M, Zhang DL (2017) Zircon U–Pb and Hf–O isotopes trace the architecture of polymetallic deposits: A case study of the Jurassic ore-forming porphyries in the Qin–Hang metallogenic belt, China. Lithos 292–293:132–145. https://doi.org/10.1016/j.lithos.2017.08.016

Zhou MF, Yan DP, Kennedy AK, Li YQ, Ding J (2002) Shrimp U-Pb zircon geochronological and geochemical evidence for neoproterozoic arc-magmatism along the western margin of the Yangtze Block, South China. Earth Planet Sc Lett 196(1–2):51–67. https://doi.org/10.1016/S0012-821X(01)00595-7

Zhou XM, Sun T, Shen WZ, Shu LS, Niu YL (2006) Petrogenesis of mesaozoic granitoids and volcanic rocks in South China: a response to tectonic evolution. Episodes 29(1):26–33. https://doi.org/10.18814/epiiugs/2006/v29i1/004

Zhou YZ, Zeng CY, Li HZ, An YF, Liang J, Lü WC, Yang ZJ, He JG, Shen WJ (2012) Geological evolution and oreprospecting targets in southern segment of Qinzhou Bay-Hangzhou Bay juncture orogenic belt, southern China. Geol Bull China 31(2/3):486–491 **(in Chinese with English abstract)**

Zhu XY, Wang JB, Wang YL, Cheng XY, Fu QB (2012) Sulfur and lead isotope constraints on ore formation of the Huangshaping W-Mo–Bi–Pb-Zn polymetallic ore deposit, Hunan Province, South China. Acta Petrol Sinica 28(12):3809–3822 **(in Chinese with English abstract)**